Check for updates

View Article Online
View Journal

NJC

Accepted Manuscript

This article can be cited before page numbers have been issued, to do this please use: G. Raveendra, C. Li, Y. Cheng, F. Meng and Z. Li, *New J. Chem.*, 2018, DOI: 10.1039/C7NJ04734G.

Volume 40 | Number 1 | January 2016 | Pages 1–846

NJC

New Journal of Chemistry
www.rsc.org/njc

A journal for new directions in chemistry

ISSN 1144-0546

ROYAL SOCIETY OF CHEMISTRY

PAPER
Jason B. Benedict et al
The role of atropisomers on the photo-reactivity and fatigue of diarylethene-based metal–organic frameworks

ROYAL SOCIETY OF CHEMISTRY

rsc.li/njc

View Article Online
DOI: 10.1039/C7NJ04734G

Direct Transformation of Syngas to Lower Olefins synthesis over Hybrid Zn-Al_2O_3/SAPO-34 Catalysts

G. Raveendra, Congming Li*, Yang Cheng, Fanhui Meng and Zhong Li*

Key Laboratory of Coal Science and Technology, Ministry of Education and Shanxi Province, Taiyuan University of Technology, Taiyuan 030024, Shanxi, China

Abstract

Syngas is a key platform chemical for the utilization of non-petroleum carbon resources. Therefore, a great attention has been paid to the syngas conversion to value added chemicals, such as lower olefins (C_2-$C_4^{=}$), liquefied petroleum gas (LPG), gasoline and aromatics. Among these value added chemicals the lower olefins is a promising chemicals, and the direct synthesis of lower olefins from syngas was investigated over a series of hybrid catalysts composed of Zn-M catalysts (M=Al_2O_3, ZrO_2, Cr_2O_3 and CeO_2) and SAPO-34 zeolite. The Zn-M catalysts and different Si/Al ratio of SAPO-34 zeolites were synthesized by co-precipitation and hydrothermal methods, respectively. The aim of the present study the influence of various supports on the catalytic performance of in this reaction. The catalysts were well characterized by X-ray diffraction (XRD), SEM, ICP-AES, BET surface area, NH_3-TPD, CO_2-TPD, FT-IR, TEM-EDS and H_2-TPR techniques. NH_3-TPD results showed that with the increase of Si/Al ratio in SAPO-34 zeolite the catalysts exhibit higher acidity due to higher amount of silica content. From the H_2-TPR and XRD results suggested that the Zn/Al_2O_3 catalyst shows strong metal support interactions it is favorable for the higher activity. Various factors that affect the catalytic activity, including reaction pressure, catalysts weight ratio, SiO_2/Al_2O_3 ratio and integration manner of both active components were investigated. These results clearly demonstrated that Si/Al ratio in SAPO-34 catalyst had a predominant effect on lower olefins selectivity. The Zn/Al_2O_3 with SAPO-34(0.043) catalyst

View Article Online
DOI: 10.1039/C7NJ04734G

showed excellent lower olefins selectivity (80%). For the integration manner of hybrid catalysts, the highest activity was obtained when the powders of both Zn/Al_2O_3 and SAPO-34 catalysts was grinded in a mortar for 10 min and pelletized. While the sequential bed and granule mixing of Zn/Al_2O_3 and SAPO-34 catalyst showed less amount of lower olefins selectivity, indicating that appropriate proximity of active components favor the lower olefins selectivity.

Keywords: Lower olefins, Syngas, Zn-Al_2O_3, SAPO-34

Corresponding authors: Congming Li; Zhong Li, Email:licongming0523@163.com;
lizhong@tyut.edu.cn

1. Introduction

The lower olefins such as ethylene, propylene and butylenes are very important chemicals and these are used in petrochemical industry as key building blocks. This can be used for to synthesize value added chemicals such as polymers, solvents and drugs. The lower olefins are mainly synthesized by catalytic cracking of naphtha, gas oil and light alkanes.[1, 2] The rapid depletion of petroleum resources that serve as the source of these hydrocarbons, there is an urgent need for the development of direct synthesis processes which can produce lower olefins from alternative feedstock's.[3, 4] The production of lower olefins is more than 120 million metric tons per year.[1] Syngas converted into lower olefins by three different routes: (1) Fischer-Tropsch (FT) Synthesis, (2) Syngs to olefins via ketene intermediate (3) Syngas to olefins via methanol intermediate. FT-Synthesis route is a well known process for the transformation of syngas to olefins synthesis. Long time onwards many scientists have studied for FT synthesis route mostly on Fe based catalysts.[5, 6] However, the lower olefins selectivity is limited because of Anderson–Schulz–Flory distribution(ASF). Another indirect route is syngas to lower olefins synthesis via dimethyl ether or methanol intermediate.[7] The production of lower olefins roared for the development of efficient and

View Article Online
DOI: 10.1039/C7NJ04734G

applicable strategies to achieve high selectivity, thermal stability and longer life time.[8, 9] Indirect synthesis route, the development of a hybrid catalyst, combining a Zn based methanol synthesis catalyst and SAPO-34 as a methanol to lower olefins synthesis catalyst, are well suited for the lower olefins synthesis, in this process first syngas converted into CH_3OH and then methanol selectively converted into lower olefins. This is a promising route for selective conversion of syngas to lower olefins synthesis in a single step process. Such a direct synthesis route could take advantage for lower olefins synthesis, as a result of high selectivity of lower olefins at lower reaction pressure.[10] Generally most of the previous publications from syngas to methanol synthesis over copper based catalysts used at lower reaction temperatures. As we well known, Cu based catalysts are sensitive to reaction temperature easy to sintering and leading to deactivation of catalyst particularly at higher reaction temperatures of >300°C.[11] Generally most of the mixed metal oxides are inactive and rarely been used for CO hydrogenation, they are mainly used as a promoters and supports for metal catalysts.[12, 13] The above mentioned drawbacks of Cu based catalysts, first Wang et.al selected Zn metal as an active site component for the one pot synthesis of lower olefins from syngas at high reaction temperatures.[18] In methanol synthesis ZnO as an active site, and the role of $Al_2O_3$was attributed to spinel formation, which can be prevented the sintering of ZnO crystallites with high surface area and better distribution of ZnO particles.[14] The direct synthesis of lower olefins ($C_2^=$–$C_4^=$) from syngas with high selectivity (>60%) is a big challenge. But recently, some of the researchers they break through the ASF distribution to achieved high selectivity of lower olefins. For eg. (1) FT-Synthesis route, Torres Galviz et al. reported that Fe based catalysts gave lower olefins ($C_2^=$–$C_4^=$)selectivity of 61%.[3] Zhong et al. found that cobalt carbide nanoprism catalysts gave lower olefins with a selectivity of 61%[15],(2) Ketene intermediate route, Zhu et al[16] reported MnO/MSAPO-34 catalyst showed the selectivity of $C_2^=$–$C_4^=$is 79.2%. Jiao et al[17] reported Zn-Cr_2O_3/SAPO-34 catalyst gave the

View Article Online
DOI: 10.1039/C7NJ04734G

selectivity of lower olefins is about 80%. (3) Methanol intermediate route, Cheng et al[18] reported Zn-ZrO_2/SAPO-34 catalyst for syngas to lower olefins synthesis the selectivity of $C_2^=$–$C_4^=$ is only 63%.

In the present work, the nano sized SAPO-34 zeotype with different Si/Al ratio was synthesized by hydrothermal method. The Zn supported catalysts were synthesized by co-precipitation method. Here we report the direct transformation of syngas to lower olefins synthesis via methanol intermediate in a fixed-bed single reactor. The 2 μm nano sized SAPO-34(0.043) zeolite with combination of Zn/Al_2O_3 as a hybrid catalyst exhibits high activity. Our intension is high activity means in terms of selectivity of the lower olefins (80%) when the conversion level of CO is low compared to the previous literature.[18] Our results also supported from the previous literature for eg. Guangrui Chen et al reported that the nano-sized SAPO-34 catalysts exhibit remarkably prolonged lifetimes and high selectivity of ethylene and propylene.[19] Qiming Sun et al reported nanosheet like SAPO-34 with lower silicon content of sample exhibited the longer catalyst lifetime and the lowest coking rate in the MTO reaction.[20] However, to the best of our knowledge, there is no work dealing with syngas to lower olefins synthesis over Zn-Al_2O_3/SAPO-34(1:2) catalysts. Our results clearly demonstrate that reducing the silicon contents of 2 μm nano sized SAPO-34(0.043) zeolite which exhibits high selectivity of lower olefins. Among the different supported Zn catalysts the Zn/Al_2O_3catalyst is synergistically interacted with SAPO-34 zeolite which exhibits high catalytic activity. These activity results were correlated with XRD, H_2-TPR, NH_3-TPD, CO_2-TPD and BET surface area.

2.0 Experimental

2.1. Chemicals

Zinc nitrate hexahydrate ($Zn(NO_3)_2$. $6H_2O$), aluminium nitrate nonahydrate $Al(NO_3)_3$. $9H_2O$) and anhydrous sodium carbonate (Na_2CO_3) were provided by Beijing reagent factory,

View Article Online
DOI: 10.1039/C7NJ04734G

China. Phosphoric acid (H_3PO_4, 85wt%,), aluminium iso-propoxide ($Al(OPri)_3$, 99.5wt%, tetraethyl ammonium hydroxide solution (TEAOH, 35wt%, Alfa Aesar), and colloidal silica (40wt%, Aldrich).

2.2 Catalyst preparation

2.2.1 Synthesis of Zn/Al_2O_3 catalyst

The weight ratio of 1:3 Zn-X (X=Al_2O_3, ZrO_2, Cr_2O_3 and CeO_2) catalysts was prepared by co-precipitation method. The required quantity of aqueous solutions containing $Zn(NO_3)_2.6H_2O$, different supported metal nitrates and Na_2CO_3 solution were simultaneously added into a 1000 ml beaker at 65°C by using peristaltic pump. The resulting solution was stirred continuously and the pH value is kept for 7.0 by adjusting the addition of two solutions. After completion of the precipitation step the obtained precipitate was aged for 2h. Then, the precipitate was filtered and washed with deionized water to remove sodium ions. The filtered cake was dried in oven at 100°C for 12 h and subsequently calcined at 400°C for 4 h in a muffle furnace.

2.2.2. Synthesis of nano-sized SAPO-34 zeolite catalysts

The SAPO-34 zeolite was synthesized by hydrothermal method reported in the previous literature.[20] The molar composition of the gels $1.0Al_2O_3$: $1.2P_2O_5$: 2.0TEAOH: $XSiO_2$: $40H_2O$ (X = 0.2, 0.4 and 0.6). In the first step aluminium isopropoxide was mixed with TEAOH (35%) solution and deionized water, after stirring the mixture until dissolved completely.Then, phosphoric acid was added drop wise and stirred for 2 h. Finally, colloidal silica (Ludox-40%) was added. The resulting mixture was further stirred for 1 h.The resulting synthesis gel was transferred into a 100 ml Teflon-lined stainless steel autoclave. The gel was crystallized in oven at 170^{o}C for 72 h. After crystallization, the slurry was washed several times with deionized water and finally washed with ethanol, dried in oven at 80^{o}C over night followed by calcination in a muffle furnace at 550^{o}C for 6 h.

View Article Online
DOI: 10.1039/C7NJ04734G

The hybrid catalysts were prepared by the following procedure. The required amounts of methanol synthesis catalyst with SAPO-34 zeolite was prepared by grinded the mixture of two powders in an agate mortar at a mass ratio of 1:2 (w/w) to form homogeneous hybrid catalyst, followed by pressing the mixture into tablets and crushed into 20-40 mesh particle size before the reaction.

2.3. Characterization

XRD pattern was recorded to determine the crystalline phase composition of the sample using German Bruker D4 X-ray diffractometer with Ni-filtered Cu Kα radiation (40 kV, 30 mA,) and the metal oxide catalysts the scan range was 2θ = 5–80° and SAPO-34 zeolites the scan range was 5-50^{o} with a scanning rate of 8°/min.

The morphology of catalysts was studied by scanning electron microscopy (SEM) on a JEOL scanning electron microscope.

FT-IR experiments were carried out in Germany BRUKER TENSOR infrared spectroscopy. The KBr pellet and the sample were mixed and ground in a mortar, the weight ratio of KBr and sample is 100: 1 for determination of functional groups in the sample.

TEM and high-resolution TEM (HRTEM) experiments were performed on a JEOL JEM-2100 electron microscope, operating at 200 kV.The powder samples were ultrasonically dispersed in ethanol at room temperature for 30 min and transferred onto a carbon-coated copper grid by dipping.

The N_2 adsorption–desorption measurements were carried out on a Micromeritics 2020 analyzer at -195.65^{o}C, after the sample was degassed at 350^{o}C under vacuum. The total surface area was calculated based on the BET equation. The micropore volume, external surface area and micropore surface area were evaluated by using the t-plot method. The total pore volume was determined from the amount adsorbed at the relative pressure of about 0.99.

View Article Online
DOI: 10.1039/C7NJ04734G

Elemental analysis was performed by inductively coupled plasma atomic emission spectroscopy (ICP-AES). 2 ml of conc HF was used to dissolved 40 mg of catalyst sample, followed by adding 2 ml of 30 wt.% H_2O_2; prior to analysis, the solution was then diluted to 1000 ml with de-ionized water. The contents of Si, Al, P and O in SAPO-34 and Zn, Al, Zr and Ce were determined.

H_2-TPR measurements were performed on Micromeritics Auto Chem 2920 instrument. Typically, 20 mg of catalyst was loaded into a U-shape quartz reactor, and sample was degasified with nitrogen gas (50 mL/min) at 300^{o}C for 30 min to remove the physisorbed moisture from the catalyst. After cooling to temperature 50^{o}C, the gas was switched to 10% H_2/Ar at a flow rate of 30 mL/min. The process was continued until a stabilized baseline was obtained in the gas chromatograph. Then, the TPR analysis was carried out from 50 to 800^{o}C with a heating rate of 10^{o}C/min. The amount of H_2 consumption was monitored by a TCD.

NH_3-TPD experiments for the surface acidity determination were performed Micromeritics Auto Chem 2920 instrument. In a typical analysis, 40 mg of the sample was loaded into a U-shaped quartz micro-reactor and pre-treated in a N_2 gas 50ml for min at 300°C for 30 min.The sample was cooled down to 50 °C and then exposed to NH_3 (15% NH_3-85% He mixture gas) for 30 min was subsequently flushed with He at the same temperature to remove physiosorbed ammonia. The process was continued until a stabilized baseline was obtained in the gas chromatograph. The TPD measurements were conducted in flowing of He gas (30 ml/min) and the temperature increasing from 50 to 800°C with a constant heating rate of 10°C/min. Thus, the spectra during desorption of NH_3 was recorded.

CO_2-TPD experiments for the surface basicity determination were performed using a conventional flow apparatus equipped with a thermal conductivity detector. In a typical analysis, 40 mg of the sample was loaded into a U-shaped quartz micro-reactor and pre-

View Article Online
DOI: 10.1039/C7NJ04734G

treated in a N_2 gas 50 ml/min at 300°C for 30 min. The sample was cooled down to100°C and then exposed to CO_2 (15% CO_2-85% He mixture gas) for 30 min, was subsequently flushed with He gas at the same temperature to remove physiosorbed CO_2.The process was continued until a stabilized baseline was obtained in the gas chromatograph. The TPD measurements were conducted in flowing He (30 ml/min) from100 to 800°C with a constant heating rate of 10°C/min. Thus, the spectra during desorption of CO_2 was recorded.

2.4 Catalytic performance test

The catalytic performance of the prepared hybrid catalysts were carried out in syngas to lower olefins synthesis. The catalytic activity test was performed in a continuous-flow, fixed-bed reactor. Typically, 0.5 g of 20-40 mesh hybrid catalyst was mixed with 0.2 g of 20-40 mesh $SiO_2$was packed into a stainless steel tubular reactor between quartz wool plugs. Prior to each test, the catalyst was reduced in-situ in a pure H_2 (30 mL/min) at 400°C for 4 h under atmospheric pressure. After reduction the reactor was cooled down to 300^{o}C, and the syngas with a H_2/CO ratio of 2/1 was introduced, raising the pressure to 1.0 MPa and the temperature of 400°C. The reaction time is fixed for 25 h. All post-reactor lines and valves were heated to 200°C to prevent product condensation. The product stream was analyzed by an online gas chromatography (Agilent 7890A), which was equipped with flame ionization detector (FID) and thermal conductivity detector (TCD), using He (99.99%) as a carrier gas.The FID detector was equipped with HP-AL/S column(30 m × 530μm × 15μm) was used to analyze CH_4 and C_{2-4} and TCD detector equipped with Porapak-Q column (2m × 3mm), HP-PLOT/Q column(30m × 530μm × 40μm) and HP-MOLESIEVE column (30m × 530μm × 25μm) were used to analyze CO, N_2 and CO_2.The temperature of FID and TCD were 300°C and 250°C, respectively. The products in the syngas to olefins are mainly as gas products. In each experiment, the balance of carbon was checked. The catalytic activity was evaluated at the steady state of reacting system.

The conversion of CO, the selectivity of CH_4, CO_2 and C_2–C_4 were calculated on a carbon-atom basis using the following equations:

The CO conversion was calculated by comparing the molar inlet and outlet flows of CO:

$$X_{CO} = \frac{F(CO_{in}) - F(CO_{out})}{F(CO_{in})} \text{ X } 100\%$$

$$S_{CH4} = \frac{F(CH_{4,\ out})}{F(CO_{in}) - F(CO_{out})} \text{ X } 100\%$$

$$S_{CO2} = \frac{F(CO_{2,\ out})}{F(CO_{in}) - F(CO_{out})} \text{ X } 100\%$$

$$S_{Cj} = \frac{j \text{ X } F(C_{j,\ out})}{F(CO_{in}) - F(CO_{out})} \text{ X } 100\% \ (j = 2, 3, 4)$$

where XCO, SCH_4, SC_j and SCO_2 refer to the conversion of CO, the selectivity of CH_4, $C_{2\text{–}4}$ and CO_2, respectively.$C_{2\text{–}4}$ represents C_2H_4, C_2H_6, C_3H_6, C_3H_8, C_4H_8, and C_4H_{10}. F represent the flow rate of CO, $C_{2\text{–}4}$, CH_4 and CO_2 (mL/min, STP), respectively. The schematic diagram of syngas to olefins synthesis diagram are shown in Fig. 1.

View Article Online
DOI: 10.1039/C7NJ04734G

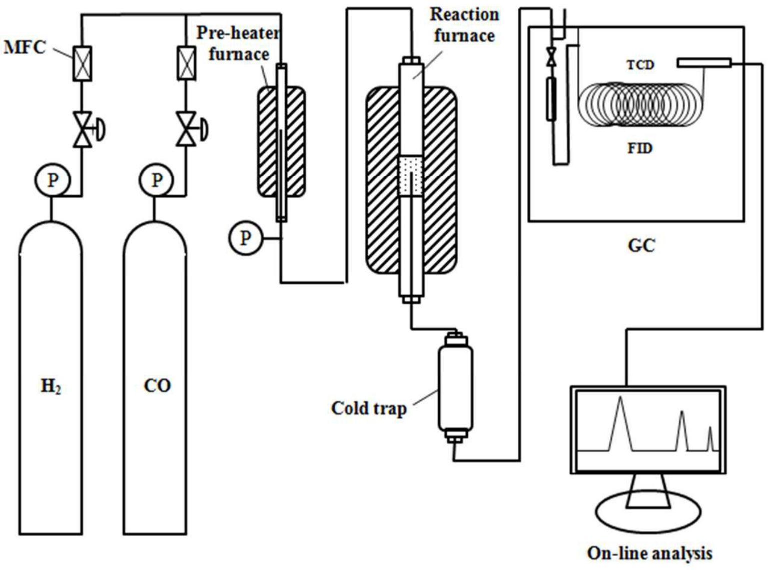

Fig. 1. The schematic diagram of syngas to lower olefins synthesis

3.0 Results and discussion

3.1 Physicochemical characterization

The chemical compositions of calcined SAPO-34 samples were determined by ICP-AES analysis and the results are presented in Table 1(a). The TEM-EDS analysis of SAPO-34 samples is shown in Fig. 2. The composition of SAPO-34 samples agree with the nominal compositions calculated from the catalyst preparation, and the content of Si/Al ratio is about 0.2 in SAPO-34(0.043), 0.4 SAPO-34(0.082) and 0.6 in SAPO-34(0.091) for all samples. From the chemical analysis, it can be seen that the Si contents in the synthesized samples from 0.2 to 0.6 are increased with the increase of silica added in the reaction mixtures. From the TEM-EDS analysis the silica content of SAPO-34(0.043) sample the weight percentage of silica is 2.88% whereas SAPO-34(0.082) sample the silica content is 5.04% and SAPO-34(0.091) sample contains the silica content is 5.94% it can be concluded that with increase of Si/Al ratio the silica content increased. The reported values for the nominal Si/Si+Al+P

View Article Online
DOI: 10.1039/C7NJ04734G

ratio actually correspond to the nominal $SiO_2/SiO_2+Al_2O_3+P_2O_5$ ratio. As a result, the reported values are in good agreement with both ICP and TEM-EDS results.

Table 1 (a). Textural properties of SAPO-34 catalysts

Catalysts	Si/(Si + P + Al)[a]	ICP-AES	Acidity (mmol/g)[b]
SAPO-34 (1)	0.091	$Si_{0.14}Al_{0.78}P_{0.62}O_2$	3.29
SAPO-34 (2)	0.082	$Si_{0.13}Al_{0.78}P_{0.67}O_2$	3.01
SAPO-34 (3)	0.043	$Si_{0.067}Al_{0.83}P_{0.62}O_2$	2.30

[a] The (Si/Si+P+Al) values obtained by ICP-AES [b]The acidity values from NH_3-TPD.

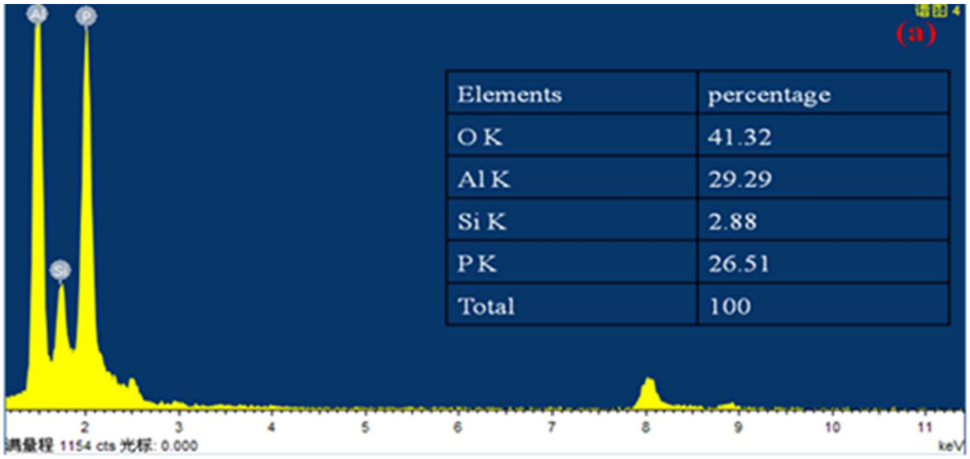

Elements	percentage
O K	41.32
Al K	29.29
Si K	2.88
P K	26.51
Total	100

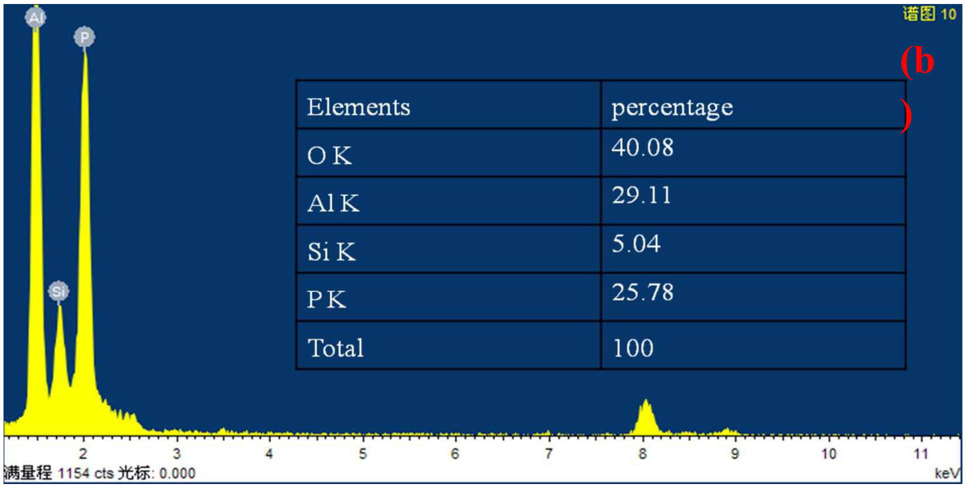

Elements	percentage
O K	40.08
Al K	29.11
Si K	5.04
P K	25.78
Total	100

View Article Online
DOI: 10.1039/C7NJ04734G

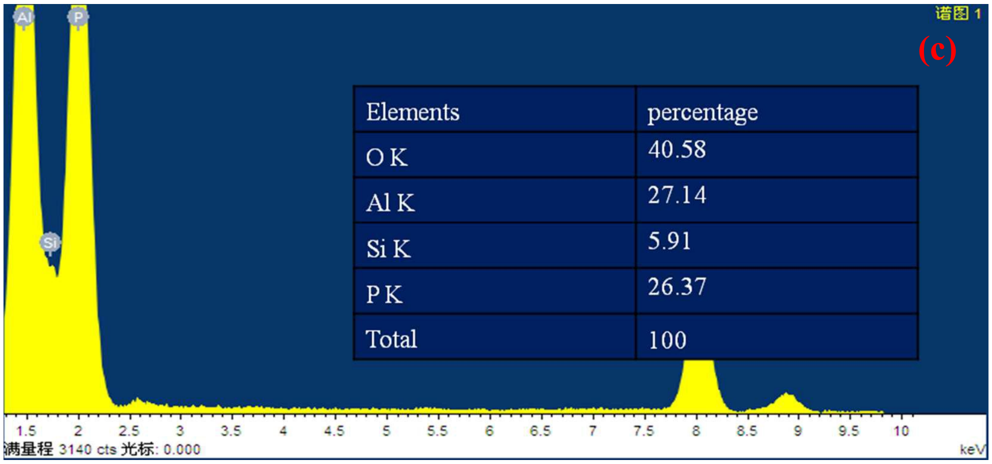

Elements	percentage
O K	40.58
Al K	27.14
Si K	5.91
P K	26.37
Total	100

Fig. 2. TEM-EDS analysis of (a) SAPO-34 (0.043) (b) SAPO-34 (0.082) (c) SAPO-34 (0.091) catalysts

The chemical compositions of Zn on three different supported catalysts were determined by ICP-AES analysis and the results are presented in Table 2. The Zn on three different supported catalysts, the theoretical weight ratio of the catalysts is fixed for 1:3 (i.e 1 for Zn and support weight ratio is 3), whereas in experimental data from the ICP-AES analysis the weight ratio value of Zn/Al_2O_3 catalysts is 1: 2.98, Zn/ZrO_2 catalyst the weight ratio is 1:2.97 and Zn/CeO_2 catalysts the weight ratio is 1: 2.98. The theoretical value is similar to the experimental value.

XRD patterns of different Si/Al ratio of SAPO-34 samples are shown in Fig. 3 (A). The main characteristic diffraction peaks of 2θ values at 9.6^o, 13^o, 15.9^o, 17.7^o, 20.7^o, 24.9^o, 26^o and 31^o are observed in the XRD of all samples, which corresponded to the chabazite structure (CHA) indicating that SAPO-34 zeolite crystals were well orderly formed.[21] All prepared SAPO-34 samples exhibit identical characteristic peaks which are in good agreement with those patterns of SAPO-34 zeolite reported in the literature. The lower Si content of SAPO-34 (0.043) sample shows lower 2θ values while with increase of silica content in SAPO-34(0.082) and SAPO-34(0.091) the peaks slightly shifted towards higher 2θ

View Article Online
DOI: 10.1039/C7NJ04734G

values as a result of change in framework composition due to the expansion/contraction of the unit cell. From the XRD results, the SAPO-34 can be prepared with TEAOH solution, no obvious impurity phase peaks is observed with increasing the amounts of silica content.

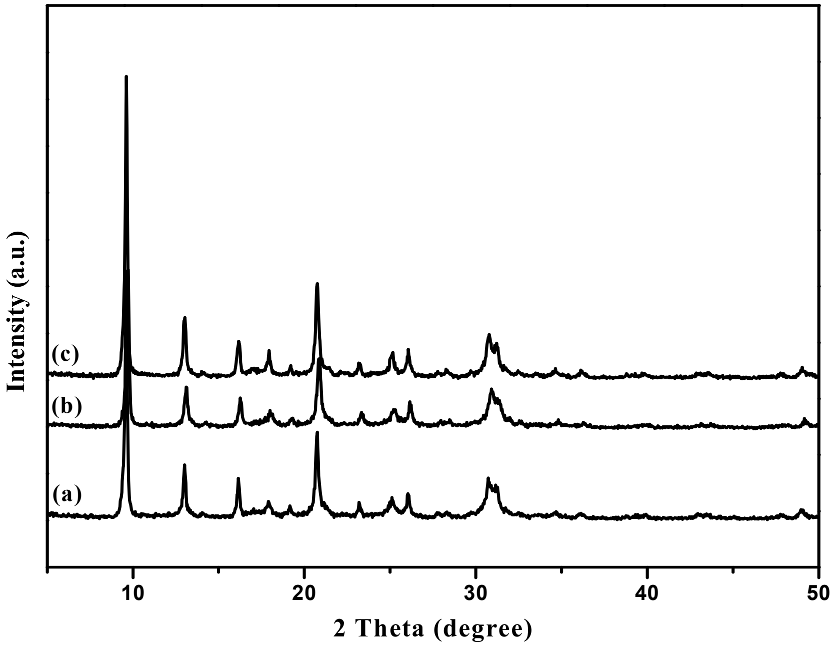

Fig.3(A). XRD patterns of (a) SAPO-34 (0.043) (b) SAPO-34 (0.082) (c) SAPO-34 (0.091) catalysts

The X-ray diffraction patterns of Zn on four different supported catalysts are shown in Fig. 3(B). The particle size of Zn on different supported catalysts was calculated by Debye Scherrer's equation and the values are presented in Table 2.

$$D= 0.94 \frac{\lambda}{FWHM_{rad}\, COS\theta}$$

where D is the average crystallite size in nm, λ= 1:54184 A˚ is the wavelength of the Cu Ka X-ray source, θ the angle under which the reflection is seen, and FWHMrad its full width at half maximum intensity in radians.[22] The Zn/Al_2O_3 catalyst shows the peaks at 2θ values of ~31.5^o, 36.6^o, 44.85^o, 49.1^o, 55.8^o, 59.5^o, 65.4^o, 74.2^o, and 77.4^o can be assigned as (220), (311), (400), (331), (422), (511), (440), (620), and (533) planes mainly attributed to the cubic structure of zinc aluminate phase.[23] There is no peaks related to the ZnO and Al_2O_3,

View Article Online
DOI: 10.1039/C7NJ04734G

indicating that Zn was uniformly dispersed on the Al_2O_3 support.[24] The Zn/Cr_2O_3 catalyst shows the diffraction peaks of 2θ = 36.0°, 54.6°, 63.4° is mainly related to the zinc chromate structure.[25] The Zn/ZrO_2 samples exhibit diffraction peaks at 2θ=30.2°, 34.8°, 50.1°, 59.8° and 62.8°, corresponding to the (111), (200), (220), (311) and (222) diffraction planes of cubic ZrO_2 phase.[26] The diffraction peaks of 31.84°, 34.75, 36.40°, 47.65°, 56.75°, 63.98°, 69.4° which are indexed to hexagonal wurtzite ZnO.[27] Whereas Zn/CeO_2 catalysts the diffraction peaks can be assigned to the (111), (200), (220), (311), (222) and (400) corresponding to a cubic fluorite structure of ceria phase.[28] From the above XRD results the Zn/Al_2O_3 catalyst the peaks shifted towards slightly higher 2θ values which are mainly attributed to the strong interaction between Zn and Al_2O_3 support which is also supported by the H_2-TPR, CO_2-TPD and NH_3-TPD results.

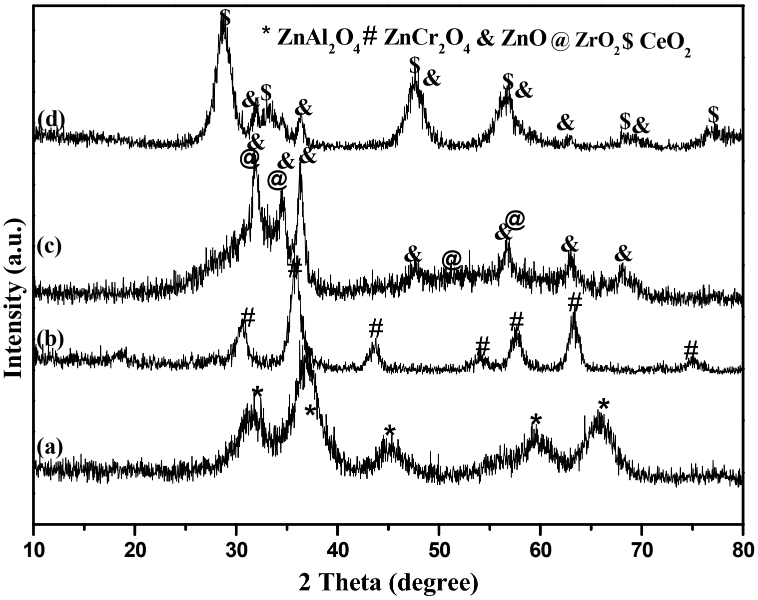

Fig. 3 (B). XRD patterns of (a) Zn/Al_2O_3 (b) Zn/Cr_2O_3 (c) Zn/ZrO_2 (d) Zn/CeO_2 catalysts

The N_2- adsorption desorption isotherms of different Si/Al ratio of SAPO-34 zeolite are shown in Fig. 4. The BET surface area, external surface areas, micropore areas, micro and mesopore volume of different Si/Al ratio of 0.2 in SAPO-34(0.043) to 0.6 in SAPO-

View Article Online
DOI: 10.1039/C7NJ04734G

34(0.091) samples are presented in Table 1(b). All of the SAPO-34 samples exhibit the characteristic type I isotherm in the curve at low relative pressures, confirming that the samples exhibit microporosity.[20] An uptake near saturation pressure in the isotherms of samples is observed due to the intercrystalline porosity, which is typical of the nanocrystal structure of SAPO-34. The BET surface area of SAPO-34 catalysts with increase of Si/Al ratio from SAPO-34 (0.043) to 0.6 SAPO-34(0.091), the surface area increased from 611 to 693 m^2/g. It can be seen that all of these samples also exhibit external surface area, which is mainly due to the some defects of the external surface as well as the intercrystalline porosity property.

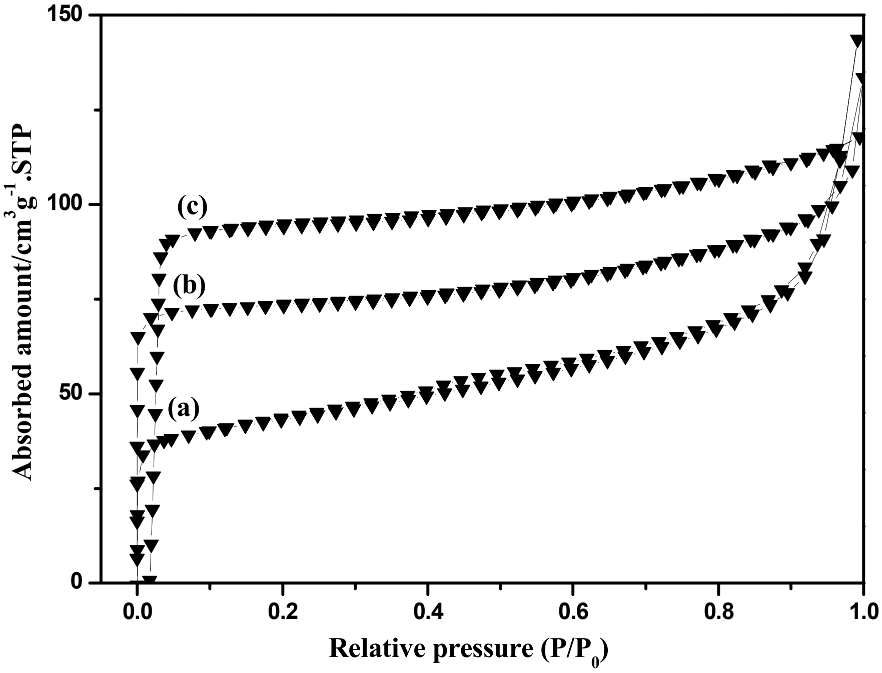

Fig.4. N_2 Adsorption-desorption isotherms of (a) SAPO-34(0.043) (b) SAPO-34(0.082) (c) SAPO-34(0.091) catalysts

View Article Online
DOI: 10.1039/C7NJ04734G

Table 1 (b).Textural properties of SAPO-34 catalysts

No.	S_{total}[a] (m^{2-1})	S_{micro}[b] (m^2 g^{-1})	S_{ext}[c] (m^2 g^{-1})	V_{micro}[c](cm^3 g^{-1})	V_{meso}(cm^3g^{-1})	V_{total}(cm^3 g^{-1})
1	611.32	553.9	57.5	0.26	0.17	0.43
2	636.53	603.2	33.4	0.26	0.05	0.31
3	693.62	650.8	42.8	0.28	0.11	0.40

[a]BET surface area [b]Smicro (micropore area), Sext (external surface area) and Vmicro (micropore volume) determined from the t-plot method. [c]Vmeso (mesopore volume) = V_{total}– V_{micro}; V_{total} is determined from the adsorbed volume at P/P0 = 0.99.

FT-IR spectroscopy is widely used technique to determine framework structures and acidity of zeolite materials. The IR spectra of SAPO-34 with varying the Si/Al ratio of samples are shown in Fig. 5. All characteristic peaks of three SAPO-34 samples are identical to those reported in the literature. In the finger print region (400–1300 cm^{-1}), the bands observed around at 490 $cm^{−1}$ and 638 $cm^{−1}$ are mainly attributed to the T-O bending bands of SiO_4 and D-6 rings. The vibration bands at 730 $cm^{−1}$ and 1095 $cm^{−1}$ are assigned to the symmetric stretching vibration of P-O (or Al-O) and asymmetric stretching vibration of O-P-O, respectively. The D-6 ring peaks correspond to the CHA framework this is key evidence for the successful synthesis of SAPO-34. The peaks at 1385 cm^{-1} and 1640 cm^{-1} corresponds to the CH_3 bending vibrations of residual template and bending vibration of water physically adsorbed on the surface of SAPO-34.[29, 21] In the hydroxyl group region (3000–4000 cm^{-1}), a broad stretching vibrational band between 3200 and 3600 cm^{-1} is attributed to the bridging hydroxyl groups, Si–OH–Al, which is responsible for the generation of Brønsted acidity of SAPO-34.[30]

View Article Online
DOI: 10.1039/C7NJ04734G

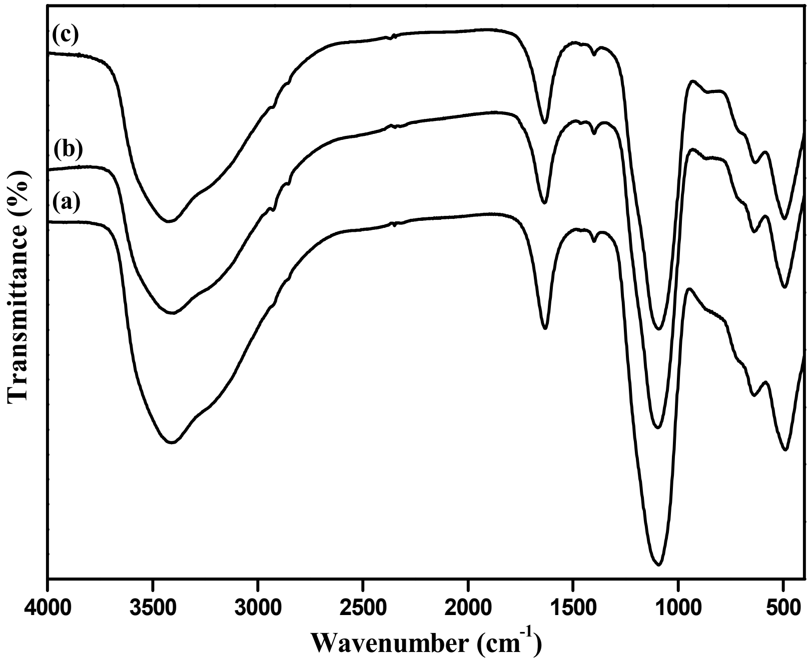

Fig.5. FT-IR spectra of (a) SAPO-34(0.043) (b) SAPO-34(0.082) (c) SAPO-34 (0.091) catalysts

NH_3-TPD technique was used to characterize the acidic properties of SAPO-34 catalysts and the results are shown in Fig. 6(A). The total acidity of the different Si/Al ratio of SAPO-34 samples is shown in Table 1(a). The desorption peak at below 100°C was associated with the physically adsorbed ammonia. All of the SAPO-34 samples exhibit two distinct peaks at two different temperatures. The first desorption peak at around150-180^{o}C is assigned to the NH_3 molecules adsorbed on weak acidic sites, which is mainly attributed to the Bronsted acid sites of P-OH groups not fully linked to the AlO_4 tetrahedra.[31] The first desorption peak area increases in the following order: SAPO-34(0.091)> SAPO-34(0.082)> SAPO-34(0.043). The intensity of high temperature desorption peak appearing at 380-410^{o}C is attributed to the strong acidic sites, which are produced by the incorporation of Si into the frame work of SAPO-34 zeolite. The SAPO-34(0.091) sample with high silica incorporation had high amount of strong acid sites probably the Si islands fabrication. From the table 1(b)

View Article Online
DOI: 10.1039/C7NJ04734G

shows the total acidity of the three different ratios of SAPO-34 catalysts, the lower Si content of SAPO-34(0.043) catalyst exhibits lower acidity with increase of Si content in SAPO-34 (0.082) and SAPO-34(0.091) the acidity of the catalysts increased.Yingxu Wei et al found that from the Si MAS NMR spectra the lower Si content of SAPO-34 sample exhibits the chemical shift value at -91 ppm, that means one Si coordination state, Si(4Al) appears in the frame work, whereas higher Si content of SAPO-34 sample with more Si incorporation which exhibits the chemical shift values of -95, 100, 105, 110 ppm. The Si incorporation into $AlPO_4$ framework by two substitution mechanisms.[32] One mechanism (SM2) is that one Si substitution for one P to form Si(4Al) entities, which gives the negatively charged framework and relatively weak Bronsted acid sites. While the double substitution of neighboring Al and P by two Si atoms (SM3) to form Si(nAl) (n = 3-0) structures leads to the formation of stronger Bronsted acid sites. The acidic strength of the bridge hydroxyl species of Si(nAl) follows in the order of Si(1Al)> Si(2Al) > Si(3Al)> Si(4Al), from the Si NMR spectra, with more Si incorporation, the increase of acid amount of SAPO-34, the acid strength may also changed. These results are correlated with our different Si/Al ratio of SAPO-34 catalysts, here the SAPO-34(0.091) sample have more acid sites and stronger acidity than other two SAPO-34 samples.[33] The NH_3-TPD results were in good agreement with the results of FT-IR spectra of samples at OH vibration band region. The Si incorporation into AlPO framework in SAPO-34 plays an important role in acid site generation.[32]

View Article Online
DOI: 10.1039/C7NJ04734G

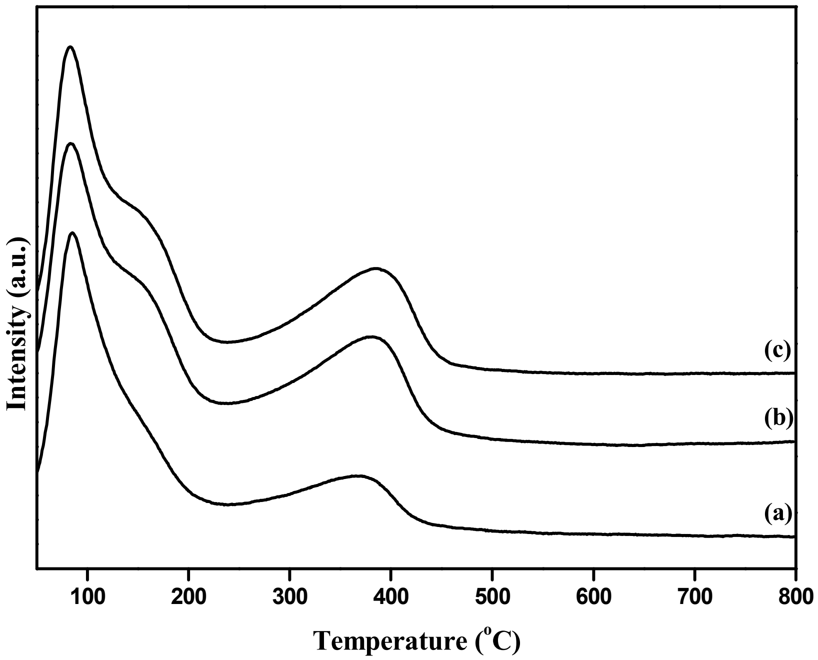

Fig.6 (A). NH_3-TPD profiles of (a) SAPO-34(0.043) (b) SAPO-34(0.082) (c) SAPO-34(0.091) catalysts

NH_3-TPD is one of the most promising techniques for characterizing the acidic property of metal oxide surfaces NH_3-TPD profiles of Zn on four different supported catalysts are shown in Fig. 6(B). The total acidity of the catalysts is presented in Table 2. According to previous literature,[34] the desorption peaks can be broadly divided into three temperature regions i.e weak (50–150°C), moderate (150–400°C), and strong (≥400°C) acidic sites. All of the catalysts show NH_3 desorption peaks in the temperature range of 100-120 °C, it is assigned to weak acidic sites of the catalysts. The Zn/Al_2O_3 catalyst shows three NH_3 desorption peaks were found at low and high temperatures region, which corresponded to the weak, moderate and strong acidic sites, respectively. Whereas in the case of Zn/Cr_2O_3 catalyst shows low and high desorption temperature regions it is also related to weak and strong acidic sites. The Zn/ZrO_2 catalyst has one high temperature desorption peak at 400-550°C it is mainly attributed to strong acidic sites. In Zn/CeO_2 catalyst shows lower and high

View Article Online
DOI: 10.1039/C7NJ04734G

desorption temperature peaks it is mainly attributed to weak and strong acidic sites. The acidity of the catalysts in Table 2 it shows that that the Zn/Al_2O_3 catalyst exhibits higher acidity when compared other supported catalysts.

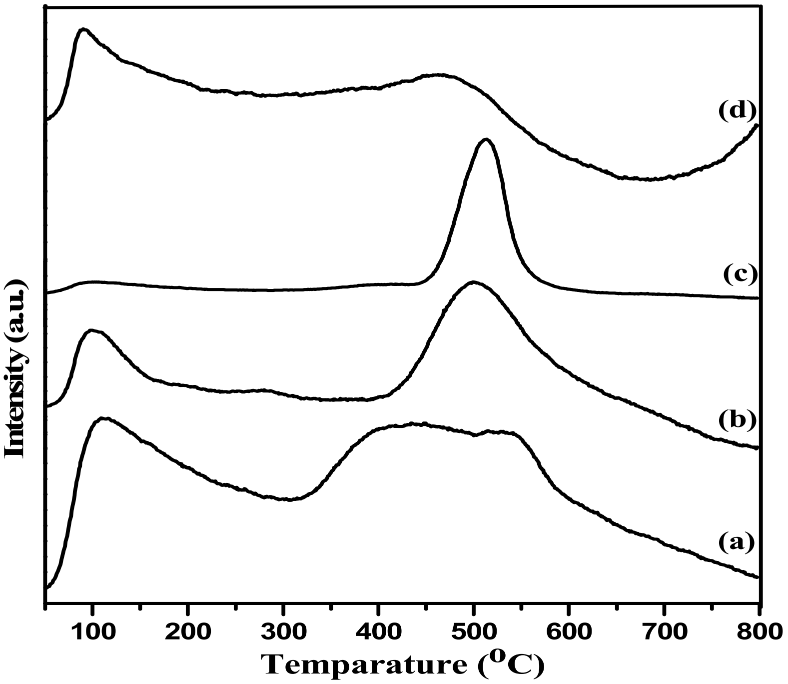

Fig. 6 (B). NH_3-TPD profiles of (a) Zn/Al_2O_3 (b) Zn/Cr_2O_3 (c) Zn/ZrO_2 (d) Zn/CeO_2 catalysts

Table 2. Textural properties of Zn on different supported catalysts

Catalysts	**Acidity (mmol/g)**[a]	**Basicity (mmol/g)**[b]	**H_2consumption (mmol/g)**[c]	**ICP-AES Zn-M**	**D (nm)**[d]
1:3 Zn/Al_2O_3	2.83	2.56	12.77	1:2.98	6.2
1:3 Zn/Cr_2O_3	1.39	1.29	4.66	-	6.4
1:3 Zn/ZrO_2	2.22	2.18	3.03	1:2.97	7.7
1:3 Zn/CeO_2	1.09	0.99	1.63	1:2.98	9.3

[a]The acidity values from NH_3-TPD,[b] basicity values from CO_2-TPD, [c]The H_2 consumption values from H_2-TPR.[d]Average particle size of the catalysts were determined by XRD using Scherrer equation

View Article Online
DOI: 10.1039/C7NJ04734G

CO_2-TPD was used to measure the basicity of metal oxide catalysts. The CO_2-TPD profiles of Zn on four different supported catalysts are shown in Fig. 6 (C). The basicity values of the catalysts are shown in Table 2. The desorption peak in the range of 100-160°C is assigned to the CO_2 interacting with weak basic hydroxyl groups on the supports. The desorption peak in the range of 160-400°C can be attributed to the association with medium basic sites, the peaks appearing above 400°C it is mainly related to the strong basic sites. The Zn/Al_2O_3 catalyst shows three CO_2 desorption peaks were found at low and high temperatures region, which corresponded to weak, moderate and strong basic sites. Whereas Zn/Cr_2O_3 catalyst shows high desorption temperature regions it is related to strong basic sites. The Zn/ZrO_2 catalyst has only high temperature desorption peak at 400-550°C it is related to strong basic sites.

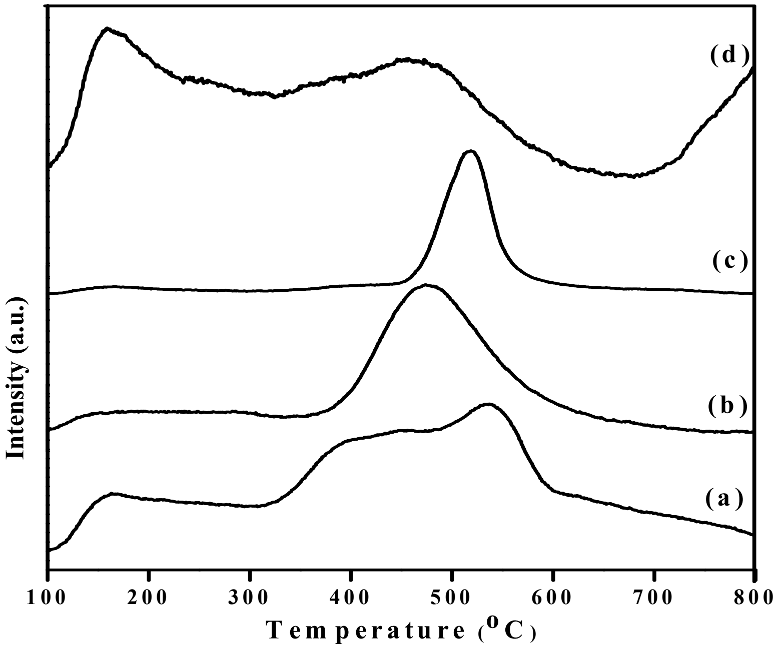

Fig. 6 (C). CO_2-TPD profiles of (a) Zn/Al_2O_3 (b) Zn/Cr_2O_3 (c) Zn/ZrO_2 (d) Zn/CeO_2 catalysts

In Zn/CeO_2 catalyst shows lower desorption peak at 100-160°C and high desorption temperature peak at 400-500°C it shows weak, moderate and strong basic sites. From the

DOI: 10.1039/C7NJ04734G

above results suggested that Zn/Al_2O_3 catalyst shows higher basicity these results also supported from the basicity values of the catalysts in Table 2.

H_2-TPR was performed to explore the reduction behavior of ZnO and the strength of metal support interaction. The Zn on different supported catalysts was characterized by H_2-TPR experiments and the results are shown in Fig. 7. The H_2 consumption values are presented in Table 2. The Zn/Al_2O_3 catalyst shows one strong reduction peak at 538°C is probably due to the ZnO surface reduction.[35] For the Zn/Cr_2O_3 catalyst, there were two hydrogen consumption peaks appearing at around 375 and 550°C.The first peak at 374°C is mainly related to the reduction of Cr^{6+} species to Cr^{3+} species, while the reduction peak at 552°C are assigned to the ZnO surface species reduction with a relatively strong interaction with the support.[36] Whereas in the case of Zn/ZrO_2 catalysts the peak at 544°C is due to the ZnO surface species reduction. Therefore in the current study, all of the Zn supported catalysts the reduction peaks mainly attributed to the ZnO surface reduction. The Zn/CeO_2 catalyst has two reduction peaks at around 430 and 750°C were observed, which can be ascribed to the reduction of surface and bulk oxygen species of CeO_2.[37] From the above results suggested that the introduction of Al ion could improves the dispersion of ZnO species and strengthen the interaction between ZnO and Al_2O_3. Among all the catalysts the Zn/Al_2O_3 catalyst leads to a shifting of the TPR peak towards to higher reduction temperature than the other three Zn supported catalysts, indicating that the stronger interactions between Zn species with the Al_2O_3 support.[38] From the Table 2 the Zn/Al_2O_3 catalyst has the consumption of hydrogen is very high when compared to other supported catalysts.

View Article Online
DOI: 10.1039/C7NJ04734G

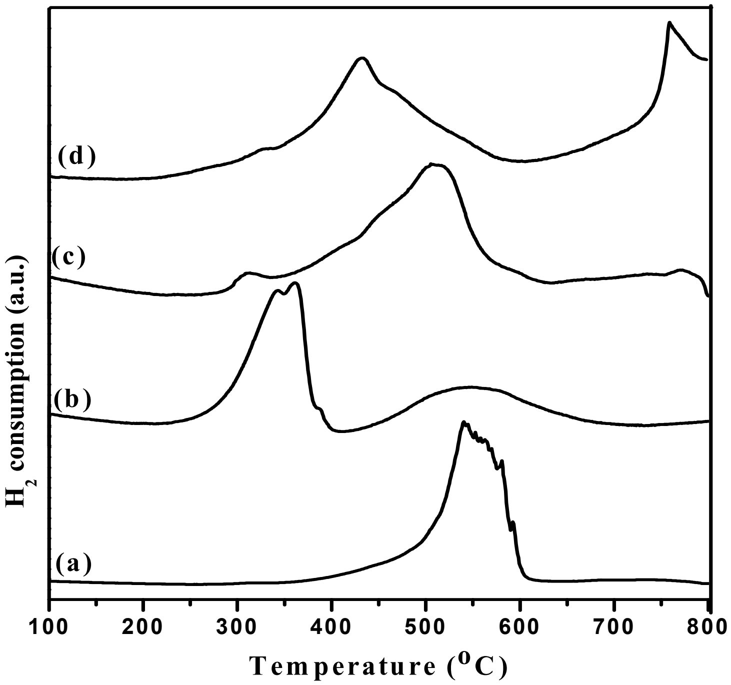

Fig. 7. H_2-TPR profiles of (a) Zn/Al_2O_3 (b) Zn/Cr_2O_3 (c) Zn/ZrO_2 (d) Zn/CeO_2 catalysts

SEM was used to find the particle size and morphology of the catalysts. The SEM images of nano sized SAPO-34 and Zn-Al_2O_3/SAPO-34 hybrid catalysts are shown in Fig. 8. It can be clearly seen that all of the SAPO-34 samples exhibit uniform nano sheet-like morphology. With increase of silica content the morphology of the catalysts changes. At lower Si/Al ratio of SAPO-34(0.043) sample the morphology is good when compared to higher Si content of SAPO-34(0.082) and SAPO-34(0.091) samples. The crystal size of all the catalysts is in the range of 2μm. The hybrid Zn-Al_2O_3/SAPO-34 catalyst the Zn/Al_2O_3 is homogeneously dispersed on the SAPO-34 it is clearly seen in the image of Fig 8(d).

View Article Online
DOI: 10.1039/C7NJ04734G

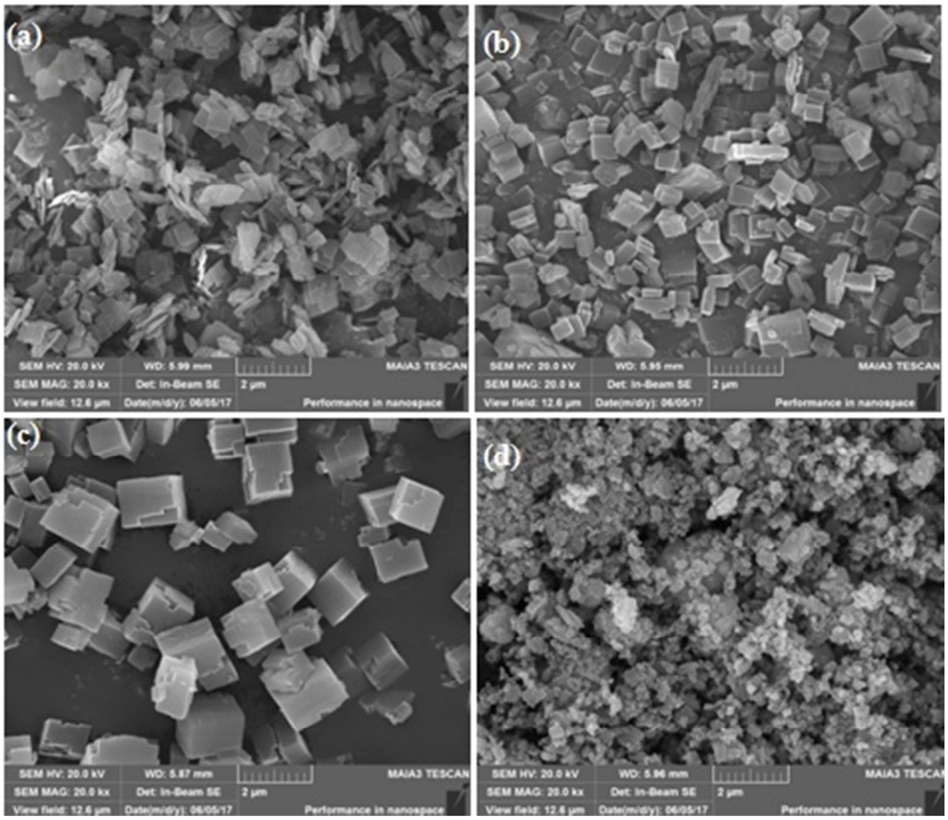

Fig. 8. SEM images of (a) SAPO-34(0.043) (b) SAPO-34(0.082) (c) SAPO-34(0.091) catalysts (d) Zn-Al_2O_3/SAPO-34 catalysts. Scale bar in (a)–(d): 2µm

3.2 Catalytic activity

3.2.1 Effect of catalysts

The catalytic activity of both Zn/Al_2O_3 and SAPO-34 zeolite experiments were done and the results were summarized in Table 3. All of the experiments in this paper the reaction time is fixed for 25 h. The blank experiments were conducted at 400 ^{o}C, 1MPa pressure and H_2/CO ratio 2:1 it showed the conversion of CO is only 0.04%. The Zn/Al_2O_3 catalyst under the same reaction conditions, the conversion of CO is very low and CH_4 as the primary product. The lower olefins selectivity is only 22%.The SAPO-34(0.043) catalyst exhibited lower CO conversion and major products belong to CH_4 and paraffins, only fewer amounts of lower olefins are formed. In both cases CH_4 is the main reaction product. The distribution of

View Article Online
DOI: 10.1039/C7NJ04734G

hydrocarbons over hybrid catalysts greatly depended on the SAPO-34 catalyst, which is affected both the CO conversion and desired hydrocarbon yields. The composite catalyst works synergistically the Zn/Al_2O_3 with SAPO-34(0.043) catalyst exhibits high activity, the CO conversion could achieved to 4.5%, and lower olefins selectivity is 77%, which is far higher than those over individual catalysts.

Table 3. Hydrogenation of CO over methanol synthesis catalysts and bifunctional catalysts composed of methanol synthesis catalyst and SAPO-34.

Catalysts	**CO conv. (%)**	**CH_4 Sel(%)**	**C_2-$C_4^{=}$ Sel (%)**	**C_2-C_4^{0} Sel (%)**	**CO_2 Sel (%)**
1:3 Zn/Al_2O_3	1.7	73.9	22.7	3.4	46.1
SAPO-34	1.00	57.9	19.8	22.3	20.7
1:3Zn-Al_2O_3/SAPO-34	4.5	10.4	77.0	12.6	44.8
1:3Zn-Cr_2O_3/SAPO-34	1.8	16	37.2	46.8	46.4
1:3Zn-ZrO_2/SAPO-34	5.3	30.2	11.2	58.6	44.4
1:3Zn-CeO_2/SAPO-34	2.1	34.4	55.8	9.8	43.6

Reaction conditions: catalyst 0.50 g; $H_2/CO=2:1$; 1 MPa; 30 $mLmin^{-1}$; time on stream 25 h; 400 ^{o}C. Selectivity was calculated on a molar carbon basis for CO hydrogenation; the formation of CO_2 by the WGS reaction. The selectivities of the products are CO_2 free.

The above results indicated that the synergistic effect existed between Zn/Al_2O_3 and SAPO-34 in the reaction of syngas to olefins synthesis. We therefore concluded that first CO hydrogenated to CH_3OH on the Zn/Al_2O_3 surface, and CH_3OH was then transformed into lower olefins on the SAPO-34 zeolite. The Zn/Al_2O_3 catalyst shows a good methanol synthesis function while SAPO-34 zeolite excellent for methanol to lower olefins due to its

View Article Online
DOI: 10.1039/C7NJ04734G

acidic sites. The maximum activity of Zn-Al_2O_3/SAPO-34 catalysts could be explained by the results obtained from XRD, FT-IR, NH_3-TPD and CO_2-TPD experiments.

3.2.2 Proximity effect of bi-functional catalysts

The proximity of the two active components in hybrid catalyst has significant influence on the catalytic activity. As shown in Fig. 9, we investigated three different types of catalytic arrangements. The use of a sequential bed filling of the catalysts with Zn/Al_2O_3 is top and SAPO-34(0.043) catalyst is below and these two catalysts were separated by a layer of inert quartz wool, the catalyst shows 2.03% of lower CO conversion is observed. The CH_4 and C_2–C_4 paraffins became the major products probably because of longer contact time of syngas with Zn/Al_2O_3 catalyst they are difficult to convert to lower olefins over the downstream bed of SAPO-34 catalyst, but lower olefins were formed because of SAPO-34 catalyst and the selectivity of olefins is 64.57%. We tried to shorten the distance between two active components further by grinding a powder mixer of both catalysts in an agate mortar to investigate the effect of their intimate contact between them. The pellets of powder mixing of Zn/Al_2O_3 and SAPO-34 hybrid catalyst is significantly increased the CO conversion to 4.5% and lower olefins selectivity of 77%, the selectivity of CH_4 is 10.4%. This is mainly due to the synergistic effect existed between Zn/Al_2O_3 and SAPO-34 catalyst. Whereas Zn/Al_2O_3 catalyst first pelletized to 20-40 mesh and SAPO-34 also pelletized to 20-40 mesh and finally both the granules of the catalysts were mixed, the distance between these two catalysts was enlarged, and methanol formed on the surface of Zn/Al_2O_3 sites, and then diffused through SAPO-34, formed methanol further converted into lower olefins, and the selectivity of lower olefins is 64.19% and the conversion of CO is 4.13%. The proximity effect of mixed oxide catalyst with SAPO-34 catalysts compared with the previous publications, the author F. Jiao et al[17] reported that the ZnCrOx-MSAPO-34 catalysts showed higher selectivity of lower olefins C_2=-C_4= (80%), obtained over the well-mixed composite catalyst of Zn/Cr_2O_3 and

View Article Online
DOI: 10.1039/C7NJ04734G

MSAPO-34 and another author K. Cheng et al[18] reported that the granule mixing of Zn/ZrO_2 and SAPO-34 catalysts exhibit higher CO conversion and high selectivity of lower olefins when compared to power mixing of Zn/ZrO_2 and SAPO-34 catalysts. Whereas in our case the powder mixing of Zn/Al_2O_3 and SAPO-34 catalyst make pellets it shows best activity for the lower olefins selectivity, this is first time reported in this work. From the above results suggested that powder mixing of hybrid catalysts gave a higher selectivity and activity for lower olefins synthesis than the other two catalysts prepared by granule mixing and sequential bed filling.

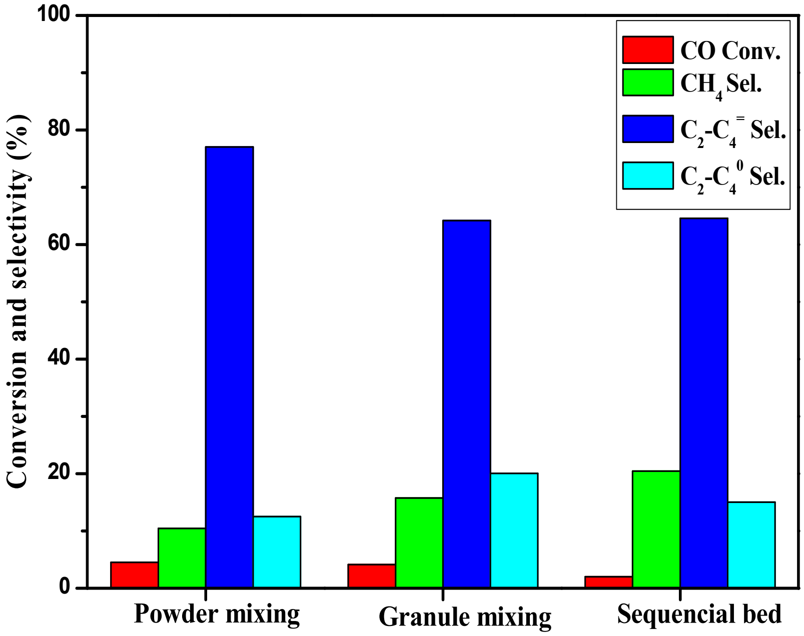

Fig. 9. Effect of catalyst mixing on syngas conversion over Zn-Al_2O_3/SAPO-34(1:2) catalysts.

3.2.3. Effect of reaction pressure

Pressure is an important parameter in syngas to lower olefins synthesis. A series of experiments were carried out to investigate the influence of reaction pressure (0.5-1.5MPa) at a constant temperature of 400°C on the catalytic performance of CO conversion and lower olefins selectivity and the results are shown in Fig. 10. At the lower reaction pressure of 0.5

View Article Online
DOI: 10.1039/C7NJ04734G

MPa the conversion of CO is 2.71% and selectivity of lower olefins is 76%. It indicates that the lower reaction pressure is not enough to increase the CO conversion. However, with the increase of reaction pressure from 0.5 to 1MPa, the conversion of CO increased to 4.5% and selectivity of lower olefins ($C_2^=$–$C_4^=$) increased to 77%. Also, the selectivity of methane is very low. When further increasing the reaction pressure from 1.0 to 1.5MPa the conversion of CO increased to 6.7% but the selectivity of lower olefins is low 62%. The increase in pressure favors the formation of CH_4 and paraffins, while $C_2^=$–$C_4^=$ formation decreased with the increase of reaction pressure. According to the thermodynamics, pressure increase in reaction it favors the equilibrium towards product side and then increase of CO conversion.[39] The above results suggested that Zn-Al_2O_3/SAPO-34 catalyst shows high catalytic performance at moderate reaction pressure of 1MPa, and this pressure is set for all of the experiments.

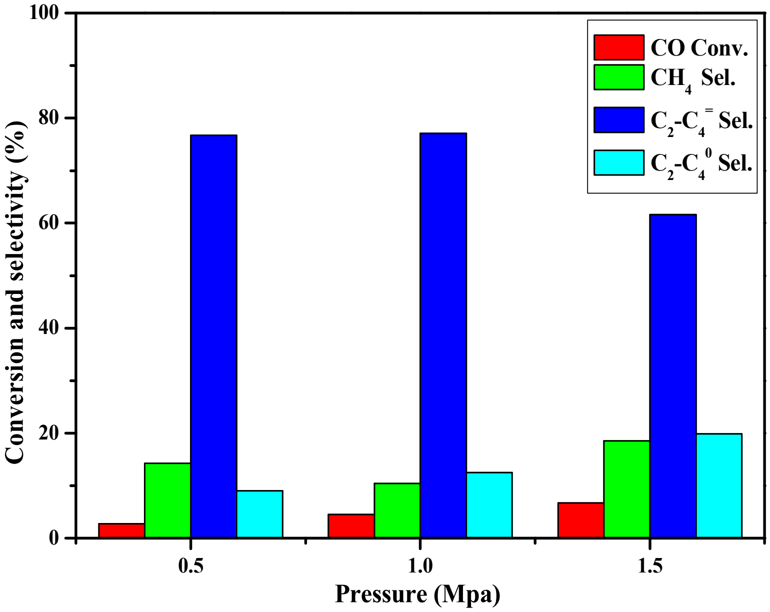

Fig. 10. Effect of pressure on syngas conversion over Zn-Al_2O_3/SAPO-34(1:2) catalysts.

View Article Online
DOI: 10.1039/C7NJ04734G

4.0 Discussion

4.1. Influence of Zn on different supported methanol catalysts

The choice of supports for lower olefins synthesis is effected by several factors such as basicity, dispersion effect and strong-metal support interactions.[40] And also important for the mechanical properties, and the interaction between active phase and supports.[41] In order to investigate the role of acidic and basic properties of supports on the catalytic performance of syngas to lower olefins synthesis, over Zn on four different supported catalysts with SAPO-34 zeolite were performed, and the results are presented in Table 3. From the reaction results, it was found that Zn-Al_2O_3/SAPO-34 catalyst gave high selectivity of lower olefins (77%) while the selectivity of methane and paraffins is low. Whereas Zn-CeO_2/SAPO-34 catalyst gave 58% selectivity of lower olefins. This is mainly due to the Zn/CeO_2 catalyst strongly interacted with the SAPO-34 and exhibits higher selectivity of lower olefins. The Zn-Cr_2O_3/SAPO-34 catalyst showed 30% selectivity of lower olefins. From the previous publications the Zn-Cr_2O_3/SAPO-34 catalyst exhibits high CO conversion (17%) and high selectivity of lower olefins at 2.5MPa, in this case the reaction proceeds through ketene intermediate. In our case the intermediate is methanol, may be differ from the CO conversion and selectivity of lower olefins, and also the interaction between Zn and Cr_2O_3 may be week. The Zn-ZrO_2/SAPO-34 catalyst gave only 10% selectivity of lower olefins and mainly it gave high selectivity of methane and paraffins. Probably; it could be ascribed to the hydrogenation property formation of olefins further hydrogenation to give paraffins. These activity results can be attributed to the different metal-support interaction, and hence to different acid-basic properties of the support. From the above results, it may be concluded that high selectivity of lower olefins obtained on Zn/Al_2O_3 catalyst, it was selected as best catalyst for the subsequent studies.

View Article Online
DOI: 10.1039/C7NJ04734G

4.2. Effect of Si/Al ratio on the catalytic performance of Zn-Al_2O_3/SAPO-34 catalysts

The catalytic activities of syngas to lower olefins synthesis over Zn-Al_2O_3/SAPO-34 hybrid catalyst and the results are shown in Fig. 11 (a). The plot of acidity vs olefins/paraffins ratio of the graph are shown in Fig. 11 (b). The CO conversion and lower olefins selectivity are strongly influenced by the Si/Al ratio in SAPO-34zeolite. The lower silica content of SAPO-34(0.043) catalyst exhibits 77% selectivity of $C_2^{=}$–$C_4^{=}$ and the conversion of CO is 4.5%. Whereas with increasing the Si/Al from 0.2 to 0.4 of SAPO-34(0.082) the conversion of CO is 4.92% but the selectivity of $C_2^{=}$–$C_4^{=}$ is varied 62.86% and when further increasing the Si/Al ratio from 0.4 to 0.6 in SAPO-34(0.091) the conversion of CO is decreased to 4.87% but the $C_2^{=}$–$C_4^{=}$ selectivity is decreased significantly to 53.73%, respectively. The selectivity of CH_4 is 17.24% and paraffins selectivity is 29.03%. Thus, higher Si content of SAPO-34 (0.091) sample, it gave higher proportion of paraffins and CH_4 formation. It is well known that Si incorporation into the AlPO framework in SAPO-34 is a key factor for acid site generation.[42] In series of SAPO-34 samples with different Si/Al ratio, the number of acid sites increased with increase of Si content for SAPO-34(0.091), as shown in Table 3. The variation of silica content indicates that lower silica content of SAPO-34(0.043) catalyst shows the best catalytic activity. This confirms that the number of acid sites is responsible for the lower olefins formation, and a lower Si content of SAPO-34(0.043) with lower surface acidity is favorable for the high selectivity of lower olefins.

View Article Online
DOI: 10.1039/C7NJ04734G

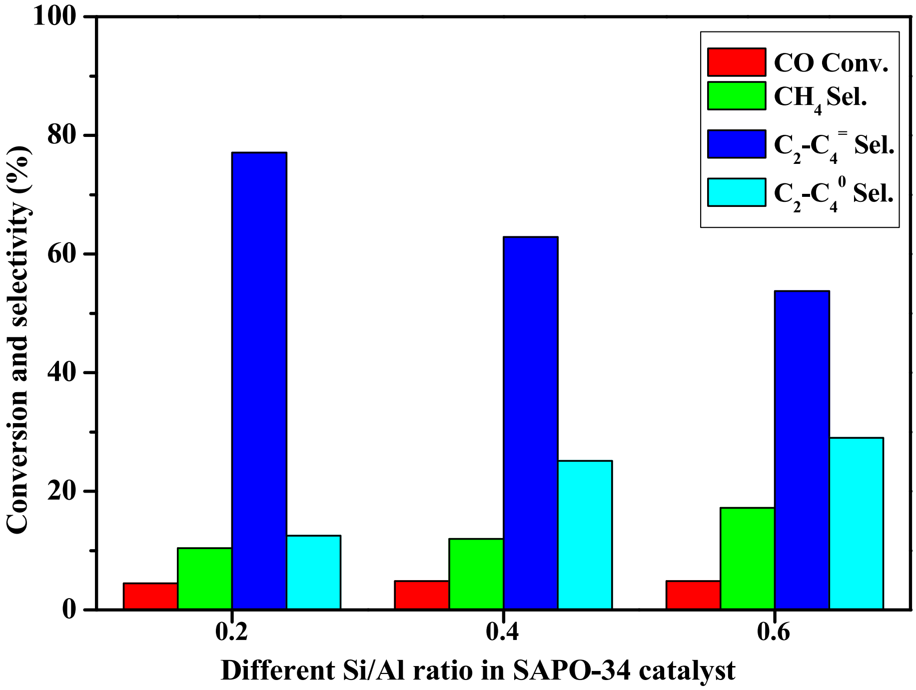

Fig. 11 (a). Effect of Si/Al ratio of SAPO-34 in Zn-Al_2O_3/SAPO-34(1:2) catalysts

The decrease in catalytic activity with increasing the Si content could be a result of several factors. The acid site concentration in SAPO-34(0.043) is lower than those in SAPO-34(0.082) and SAPO-34(0.091); hence, coke formation is slower in SAPO-34(0.043) sample so it shows higher olefins selectivity when compared to other two SAPO-34 samples. The higher number of acid sites, higher the rate of coke formation, with consequent deactivation due to coke formation in the pores of SAPO-34 zeolite.[43]

View Article Online
DOI: 10.1039/C7NJ04734G

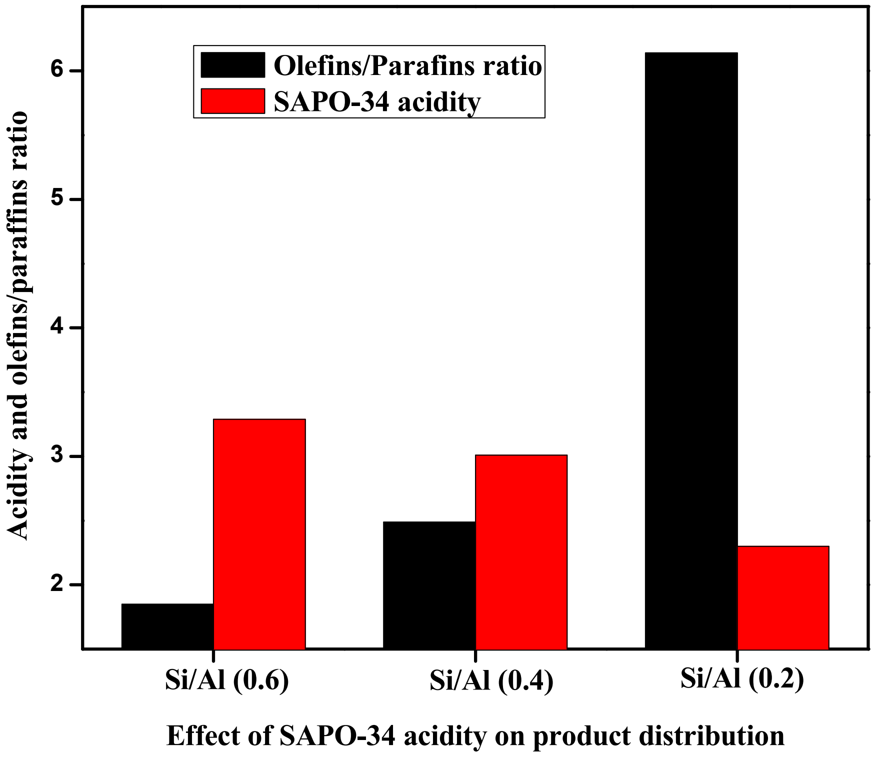

Fig. 11 (b) olefins/paraffins Vs SAPO-34 acidity

The SAPO-34 acidity comparison with the olefins/paraffins ratio is shown in Fig. 11 (b). With the increase of Si/Al ratio in SAPO-34 catalyst the olefins/paraffins ratio decreased. Among the different Si/Al ratio of the catalysts the lower Si/Al ratio of 0.2 SAPO-34 (0.043) catalyst shows higher olefins/paraffins ratio. Our results also compared with the previous literature, Qiming Sun et al reported that from methanol to lower olefins synthesis using nano sized SAPO-34 catalysts, here with increase of Si/Al ratio the lower olefins selectivity decreased. The SAPO-34 with lowest silicon content of the sample exhibited the longest catalyst lifetime and the lowest coking rate in the methanol to olefins (MTO) reaction.[20]

4.3. Effect of weight ratio between Zn/Al_2O_3 and SAPO-34 catalysts

The interaction between methanol synthesis catalyst (Zn/Al_2O_3) and SAPO-34(0.043) zeolite such as hybrid catalyst (Zn-Al_2O_3/SAPO-34) played a key role in CO conversion and lower olefins selectivity and the results are shown in Fig. 12. The results indicate that a

View Article Online
DOI: 10.1039/C7NJ04734G

significant changes in the product of lower olefins selectivity. Three different weight ratios of catalysts were tested for syngas to lower olefins synthesis. The weight ratio of Zn-Al_2O_3/SAPO-34(1:1) catalyst shows higher conversion of CO (6.3%) and the $C_2^=$–$C_4^=$ selectivity of 74% was obtained, but the selectivity of CH_4 is high 12.5%. The Zn content is favorable for high CO conversion and SAPO-34 for high olefins formation but slightly higher amount of CH_4 is formed. With increasing the catalyst weight ratio from 1:1 to 1:2 in Zn-Al_2O_3/SAPO-34(1:2) catalyst gave 4.5% CO conversion with high selectivity of lower olefins (77%). It indicated that a suitable weight ratio of Zn/Al_2O_3 to SAPO-34 could accomplish the highest selectivity of lower olefins due to the synergistic effect existing between the two catalysts during the reaction process.[44] When further increasing the catalyst weight ratio from 1:2 to 1:3 (Zn-Al_2O_3/SAPO-34) the conversion of CO is 4.95% and the selectivity of $C_2^=$–$C_4^=$ is only 55% and unusually higher amount of methane and paraffins was observed, suggesting that methanol may decompose on the surface of SAPO-34 catalyst forming CO and H_2 which in turn undergo hydrogenation to form methane.[45] Alexey V. Kirilin et al found that from syngas to lower olefins synthesis during this process formation of methanol it further hydrogenation to form methane over metallic sites. With the increase of SAPO-34 fractions from 50 to 75 vol% in Cu-Zn/SAPO-34 catalyst the C_3/C_2 ratio relatively unchanged (1.23 and 1.19). In contrast, the SAPO-34 fraction increases from 50% to 75 vol% the C_3/C_2 ratio increases from 1.5 to 2.1 in the Cr–Zn system.[46] The discrepancy of the results varied from the Alexey catalyst, these results are under investigation then we can find the exact reason. From the above results indicate that a steady increase in lower olefins selectivity up to a catalyst weight ratio of 1:1 to 1:2 ratio and then decreased the lower olefins selectivity to 55%. The weight ratio of Zn-Al_2O_3/SAPO-34 (1:2) catalyst shows high selectivity of lower olefins (77%) and also the selectivity of CH_4 is suppressed to 10.4% when compared to the

View Article Online
DOI: 10.1039/C7NJ04734G

other two weight ratio of catalysts, so we selected the weight ratio of 1:2 is the best ratio for all experiments.

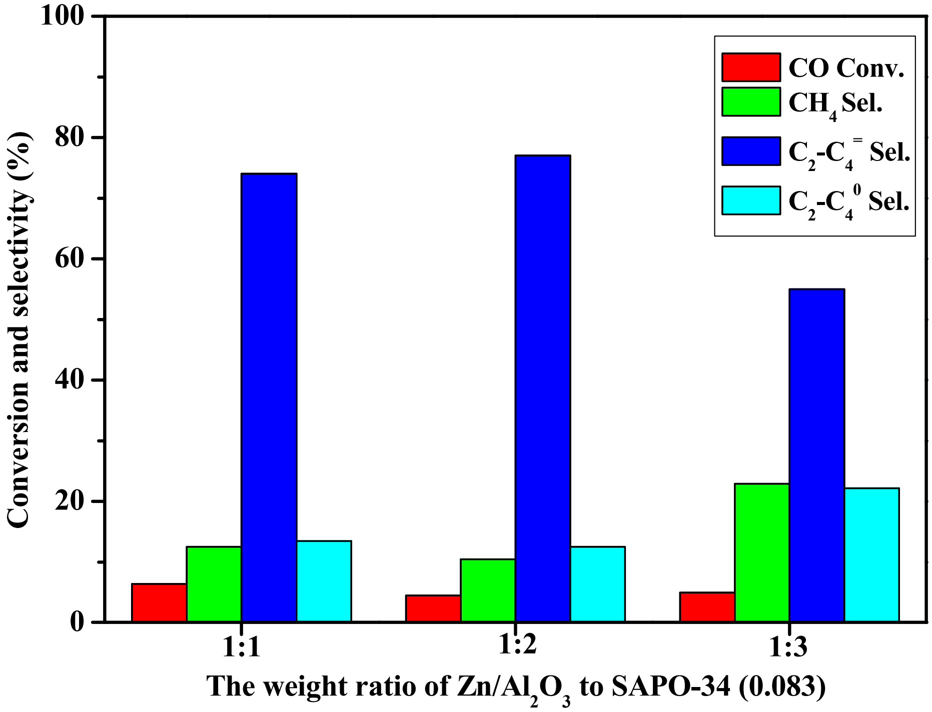

Fig. 12. The weight ratio of Zn/Al_2O_3 to SAPO-34 catalysts

4.4 Catalyst stability test

The effect of time on stream on lower olefins selectivity for the $Zn\text{-}Al_2O_3$/SAPO-34 hybrid catalysts and the results are shown in Fig. 13. With time on stream the lower olefins ($C_2^{=}$–$C_4^{=}$) formation reached to maximum selectivity of 80% at around 6 h of reaction time and further increase of reaction time the lower olefins selectivity in the product decreased to 67% at 100 h of reaction time. Over the same time, CH_4 and paraffins ratio in the product steadily increased. The decrease in selectivity with time on stream it is mainly due to the SAPO-34 zeolite is quickly coke formation in the cages, so the active sites is decreased at the same time formation of olefins further hydrogenation to form paraffins. From the previous literatures Haw and co-workers [47] found that during the conversion of methanol to olefins synthesis with time on stream phynanthrene derivatives of pyrene formed as a coke on the

View Article Online
DOI: 10.1039/C7NJ04734G

cages of SAPO-34 zeolite. The higher stability of the Zn-Al_2O_3/SAPO-34 catalysts is mainly attributed to the synergistic effect between both the catalysts and stronger metal-support interaction in Zn/Al_2O_3 catalyst. The Zn-Al_2O_3/SAPO-34 is a promising hybrid catalyst for commercial applications in direct synthesis of lower olefins from syngas.

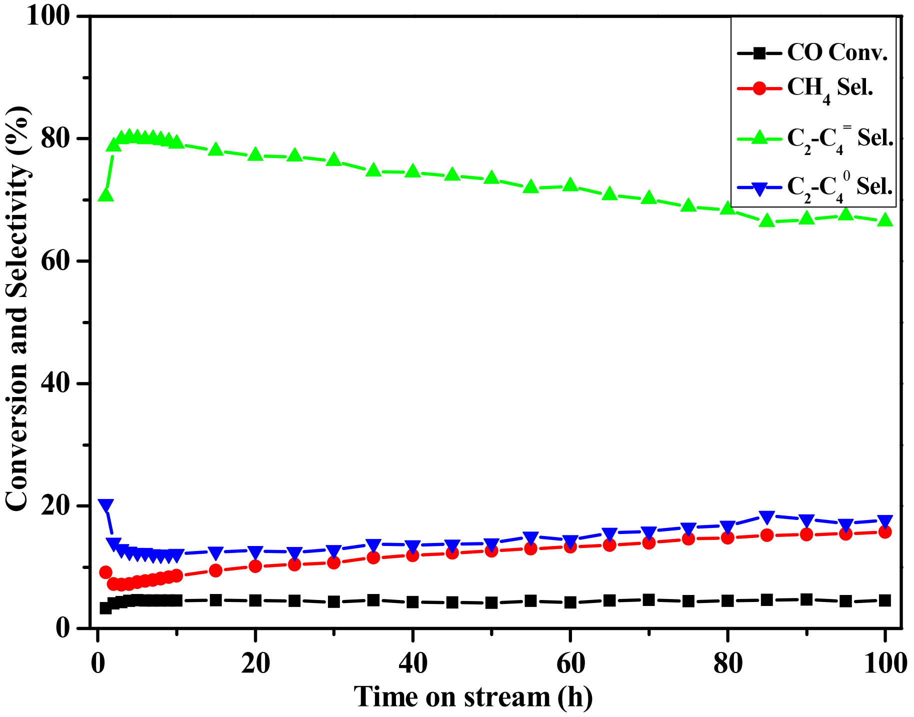

Fig. 13. Stability test over Zn-Al_2O_3/SAPO-34(1:2) catalysts.

5.0 Conclusions

The effect of various supported catalysts had a significant influence on the physico-chemical properties and catalytic performance of lower olefins synthesis. Among the various supported catalysts were studied, Zn/Al_2O_3 catalysts have been found to exhibit superior catalytic performance for methanol synthesis. We assumed that from the XRD results the particle size of the $ZnAl_2O_4$ is 6.2 nm so the Zn species is highly dispersed on alumina support. From the XRD and H_2-TPR results suggested that strong metal support interaction between Zn and Al_2O_3 can result in the formation of zinc aluminate species. The synergistic

View Article Online
DOI: 10.1039/C7NJ04734G

effect between Zn/Al_2O_3 and SAPO-34 components, which are largely improved the catalytic activity. The lower silica content of SAPO-34(0.043) is favorable for the high selectivity of lower olefins. The catalysts showed noticeable deactivation with time on stream, this is mainly due to the coke formation on the cages of SAPO-34. Our main objective is the selectivity of lower olefins with constant stability on time on stream and conversion of CO also will increase. To further improve the catalytic performance of these catalytic systems for methanol synthesis, an effective metal promoter is needed to enhance the Zn particle dispersion and reducibility, thus giving rise to higher CO conversion. At the same time the addition of structural promoters into SAPO-34 to suppress the coke formation of active phases during time on stream and to improves longer life of the catalysts.

Acknowledgements

We thank the National Science Foundation of China (Grant U1510203) for financial support.

View Article Online
DOI: 10.1039/C7NJ04734G

References

1. H. M. Torres Galvis and K. P. de Jong, *ACS Catalysis*, 2013, **3**, 2130-2149.
2. A. Corma, F. V. Melo, L. Sauvanaud and F. Ortega, *Catalysis Today*, 2005, **107**, 699-706.
3. H. M. Torres Galvis, J. H. Bitter, T. Davidian, M. Ruitenbeek, A. I. Dugulan and K. P. de Jong, *Journal of the American Chemical Society*, 2012, **134**, 16207-16215.
4. A. C. J. Koeken, H. M. Torres Galvis, T. Davidian, M. Ruitenbeek and K. P. de Jong, *Angewandte Chemie International Edition*, 2012, **51**, 7190-7193.
5. J. Lu, L. Yang, B. Xu, Q. Wu, D. Zhang, S. Yuan, Y. Zhai, X. Wang, Y. Fan and Z. Hu, *ACS Catalysis*, 2014, **4**, 613-621.
6. X. Zhou, J. Ji, D. Wang, X. Duan, G. Qian, D. Chen and X. Zhou, *Chemical Communications*, 2015, **51**, 8853-8856.
7. U. Olsbye, S. Svelle, M. Bjørgen, P. Beato, T. V. W. Janssens, F. Joensen, S. Bordiga and K. P. Lillerud, *Angewandte Chemie International Edition*, 2012, **51**, 5810-5831.
8. M. Janardanarao, *Industrial & Engineering Chemistry Research*, 1990, **29**, 1735-1753.
9. H. Yang, L. Fu, L.Wei, J. Liang, and Bernard P. Binks, J. Am. Chem. Soc., 2015, **137,** 1362-1371.
10. F. Pontzen, W. Liebner, V. Gronemann, M. Rothaemel and B. Ahlers, *Catalysis Today*, 2011, **171**, 242-250.
11. R. Fan, M. Kyodo, L. Tan, X. Peng, G. Yang, Y. Yoneyama, R. Yang, Q. Zhang and N. Tsubaki, *Fuel Processing Technology*, 2017, **167**, 69-77.
12. A. Dinse, M. Aigner, M. Ulbrich, G. R. Johnson and A. T. Bell, *Journal of Catalysis*, 2012, **288**, 104-114.
13. K. An, S. Alayoglu, N. Musselwhite, S. Plamthottam, G. Melaet, A. E. Lindeman and G. A. Somorjai, *Journal of the American Chemical Society*, 2013, **135**, 16689-16696.
14. H. Song, D. Laudenschleger, J. J. Carey, H. Ruland, M. Nolan and M. Muhler, *ACS Catalysis*, 2017, **7**, 7610-7622.
15. L. Zhong, F. Yu, Y. An, Y. Zhao, Y. Sun, Z. Li, T. Lin, Y. Lin, X. Qi, Y. Dai, L. Gu, J. Hu, S. Jin, Q. Shen and H. Wang, *Nature*, 2016, **538**, 84-87.
16. Y. Zhu, X. Pan, F. Jiao, J. Li, J. Yang, M. Ding, Y. Han, Z. Liu and X. Bao, *ACS Catalysis*, 2017, **7**, 2800-2804.
17. F. Jiao, J. Li, X. Pan, J. Xiao, H. Li, H. Ma, M. Wei, Y. Pan, Z. Zhou, M. Li, S. Miao, J. Li, Y. Zhu, D. Xiao, T. He, J. Yang, F. Qi, Q. Fu and X. Bao, *Science*, 2016, **351**, 1065-1068.
18. K. Cheng, B. Gu, X. Liu, J. Kang, Q. Zhang and Y. Wang, *Angewandte Chemie International Edition*, 2016, **55**, 4725-4728.
19. Guangrui Chen, Qiming Sun and Jihong Yu, *Chem. Commun.,* 2017, **53**, 13328--13331
20. Q. Sun, Y. Ma, N. Wang, X. Li, D. Xi, J. Xu, F. Deng, K. B. Yoon, P. Oleynikov, O. Terasaki and J. Yu, *Journal of Materials Chemistry A*, 2014, **2**, 17828-17839.
21. P. R. H. P. Rao and M. Matsukata, *Chemical Communications*, 1996, DOI: 10.1039/CC9960001441, 1441-1442.
22. D. Gruber, F. Kraus, and J. M¨uller, Sensors and Actuators B, vol. 92, no. 1-2, pp. 81–89, 2003
23. S. Battiston, C. Rigo, E. d. C. Severo, M. A. Mazutti, R. C. Kuhn, A. Gündel and E. L. Foletto, *Materials Research*, 2014, **17**, 734-738.
24. J. Agrell, H. Birgersson, M. Boutonnet, I. Melián-Cabrera, R. M. Navarro and J. L. G. Fierro, *J. Catal.*, 2003, **219**, 389-403.
25. F. Ma, S. Chen, H. Zhou, Y. Li and W. Lu, *RSC Advances*, 2014, **4**, 40776-40781.
26. Y. Esqueda-Barrón, M. Herrera, S. Camacho-López, Applied Surface Science, doi: https://doi.org/10.1016/j.apsusc. 2018.01.081
27. B. Liu and R. T. Baker, *Journal of Materials Chemistry*, 2008, **18**, 5200-5207.
28. P. Periyat, F. Laffir, S. A. M. Tofail and E. Magner, *RSC Advances*, 2011, **1**, 1794-1798.

View Article Online
DOI: 10.1039/C7NJ04734G

29. Z. Li, J. Martinez-Triguero, P. Concepcion, J. Yu and A. Corma, *Physical Chemistry Chemical Physics*, 2013, **15**, 14670-14680.
30. E. Aghaei and M. Haghighi, *Journal of Porous Materials*, 2015, **22**, 187-200.
31. B. Parlitz, E. Schreier, H. L. Zubowa, R. Eckelt, E. Lieske, G. Lischke and R. Fricke, *Journal of Catalysis*, 1995, **155**, 1-11.
32. S. Svelle, S. Aravinthan, M. Bjoregen, K.-P. Lillerud, S. Kolboe, I.M. Dahl and U. Olsbye,*Journal of Catalysis,* 2006, **241** 243
33. Yingxu Wei, Dazhi Zhang, Yanli He, Lei Xu, Yue Yang, Bao-Lian Su, and Zhongmin Liu, *Catalysis Letters*, 2007,**114**, 30-35
34. M. G. Álvarez, M. Plíšková, A. M. Segarra, F. Medina and F. Figueras, *Applied Catalysis B: Environmental*, 2012, **113**, 212-220.
35. S. Derrouiche, C. La Fontaine, G. Thrimurtulu, S. Casale, L. Delannoy, H. Lauron-Pernot and C. Louis, *Catalysis Science & Technology*, 2016, **6**, 6794-6805.
36. S. Tian, S. Ding, Q. Yang, H. Ren, Q. Ma, Y. Zhao and Z. Miao, *RSC Advances*, 2017, **7**, 20135-20145.
37. T.-Y. Ma, Z.-Y. Yuan and J.-L. Cao, *European Journal of Inorganic Chemistry*, 2010, **2010**, 716-724.
38. G. Wu, C. Zhang, S. Li, Z. Huang, S. Yan, S. Wang, X. Ma and J. Gong, *Energy & Environmental Science*, 2012, **5**, 8942-8949.
39. S. Liu, R. Ohnishi and M. Ichikawa, *Journal of Catalysis*, 2003, **220**, 57-65.
40. H. Brumberger, F. DeLaglio, J. Goodisman, M. G. Phillips, J. A. Schwarz and P. Sen, *Journal of Catalysis*, 1985, **92**, 199-210.
41. J. J. H. B. Sattler, J. Ruiz-Martinez, E. Santillan-Jimenez and B. M. Weckhuysen, *Chemical Reviews*, 2014, **114**, 10613-10653.
42. M. Ghavipour, A. S. Mehr, Y. Wang, R. M. Behbahani, S. Hajimirzaee and K. Bahrami, *RSC Advances*, 2016, **6**, 17583-17594.
43. Z. Zhu, M. Hartmann and L. Kevan, *Chemistry of Materials*, 2000, **12**, 2781-2787.
44. C. Li, H. Ban, W. Cai, Y. Zhang, Z. Li and K. Fujimoto, *Journal of Saudi Chemical Society*, 2017, **21**, 974-982.
45. D. R. Dubois, D. L. Obrzut, J. Liu, J. Thundimadathil, P. M. Adekkanattu, J. A. Guin, A. Punnoose and M. S. Seehra, *Fuel Processing Technology*, 2003, **83**, 203-218.
46. Alexey V. Kirilin, Joseph F. Dewilde, Vera Santos, Adam Chojecki, Kinga Scieranka,and Andrzej Malek, *Ind. Eng. Chem. Res,* 2017, **56**, 13392–13401
47. J. F. Haw, W. Song, D. M. Marcus and J. B. Nicholas, *Accounts of Chemical Research*, 2003, **36**, 317-326.